https://doi.org/10.3311/PPci.37021

Periodica Polytechnica Civil Engineering

Study on the Pile-soil Interaction of Large-diameter Piles Under the Wave Loading

Chong Zhao[1*], Chengchao Guo[1,2,3,4,5]

[1] School of Civil Engineering, Sun Yat-sen University, University Road 2, 519082 ZhuHai, China
[2] Southern Marine Science and Engineering Guangdong Laboratory (Zhuhai), University Road 2, 519082 ZhuHai, China
[3] Guangdong Key Laboratory of Oceanic Civil Engineering, Xingang Xi Road 135, 510275 Guangzhou, China
[4] Guangdong Research Center for Underground Space Exploitation Technology, Xingang Xi Road 135, 510275 Guangzhou, China
[5] Southern Institute of Infrastructure Testing and Rehabilitation Technology, Yanda Road 46, 516007 Huizhou, China
[*] Corresponding author, e-mail: sysuzc@163.com

Received: 01 April 2024, Accepted: 02 December 2024, Published online: 03 January 2025

Abstract

Large-diameter pile is the main foundation type of offshore wind power engineering, which needs to withstand the long-term wave loadings. The pile-soil interaction is of great significance to the safety and stability of the foundation. In this study, numerical analyses with a two-dimensional model were employed to simulate the wave loading pile in layered soils. The results revealed that the pile-soil interaction shows a positive correlation with the wave loading, present a reciprocal trend, the displacement ranging from −9.3 mm to 10.7 mm in front of the pile and from −9.7 mm to 10.4 mm behind it, the plastic strain initially arises in the soil proximate to the point of rotation, rather than at the mudline, primarily occurs in the clay layer, gradually progressing from the bottom upward and expanding outward. The soil maximum stress is 23.9 kPa in sand layer, while 15.2 kPa in the clay layer, the stress does not correlate with depth in the clay layer, but significantly influenced by the clay layer's distribution.

Keywords

monopile, wave loadings, pile-soil interaction, soil responses

1 Introduction

In recent years, the extensive development of global offshore wind power has offered an efficient solution to the pressing issues of energy scarcity and environmental pollution. The monopile foundation, a commonly employed structure in the offshore wind turbine sector, comprises 80.8% of the total foundations used, with typical diameters ranging from 6 m to 10 m [1]. These piles, which differ significantly from those used inland, are subjected to considerable and complex oceanic dynamic loadings [2]. Wave action constitutes the primary loading mode for large-diameter piles, while the Morison equation serves as the principal method used to calculate wave loading on these piles [3], it has the advantage of simple form and higher accuracy [4–6], previous studies have typically simplified the issue by considering unidirectional, bidirectional, or multidirectional horizontal cyclic concentrated loads acting on the pile [7, 8]. The effect of waves on the pile-soil interaction is primarily manifested in two aspects: firstly, waves impose horizontal loads on the pile; secondly, they directly impact the seabed, thereby inducing additional compressive stresses and superhydrostatic pore pressure on its surface. Asumadu et al. [9–11] and Zhao et al. [12] established two-dimensional and three-dimensional model to study the seabed response under the wave action, respectively. Wang et al. [13] obtained the expressions of excess pore pressure and effective stresses of seabed soil under the wave loadings. Abhinav and Saha [14] investigated the jacket response in loose sand under the wave effects, Guo et al. [15] introduced a coupled model to investigate both the seabed's dynamic resilience and the pile's mechanical behavior under wave action. Liu et al. [16] conducted an analysis of the temporal evolution of horizontal stress and displacement characteristics in soil surrounding piles subjected to wave loading.

The above research primarily delves into the impacts of wave action on the seabed and the pile displacement and deformation. Furthermore, most of these loads rely solely on a single soil layer, the pile-soil interaction in layered

Cite this article as: Zhao, C., Guo, C. "Study on the Pile-soil Interaction of Large-diameter Piles Under the Wave Loading", Periodica Polytechnica Civil Engineering, 2025. https://doi.org/10.3311/PPci.37021

soils is relatively limited. In addition, the diameter of the field test piles does not exceed 2.5 m currently, necessitating the investigation of the bearing characteristics of oversized monopiles with a diameter of 6 m under wave loading. This paper integrates the calculation method of wave force, investigates the characteristics of pile-soil interaction under wave loading, and derives the response of soil surrounding piles under such conditions. It provides valuable insights and reference specifically for the design and construction of coastal and offshore engineering structures.

2 Theory and methods of wave force calculation

2.1 The determination of wave force

The Morison equation is now widely used in engineering to calculate the wave force carried by structures with small scales, the schematic presented in Fig. 1, assuming that the pile's existence does not influence the wave characteristics [17]. The monopile can be viewed as upright pilings submerged in water, the diameter is much smaller than the wavelength, linear wave theory is used in the analyses and calculations. The wavefront equation for a linear wave as shown in the Eq. (1), substituting this into the Morison equation, obtain the wave force, as shown in the Eq. (2):

$$\eta = \frac{H}{2}\cos\left(kx-\omega t\right), \tag{1}$$

$$F = \frac{1}{2}\rho C_D D\left|u_w\right|\times u_w + \rho C_m \frac{\pi D^2}{4}\dot{u}_w, \tag{2}$$

where ρ, C_D, D, u_w, C_M is fluid density, drag coefficient, pile diameter, velocity, inertia coefficient.

The horizontal velocity of water quality point movement at any height of z is expressed as:

$$u_w = \frac{\partial \varphi}{\partial x} = \frac{\pi H}{T}\frac{\cosh k\left(z+d\right)}{\sinh kd}\cos\left(kx-\omega t\right), \tag{3}$$

where H is the wave height, k is wave number, T is the wave period.

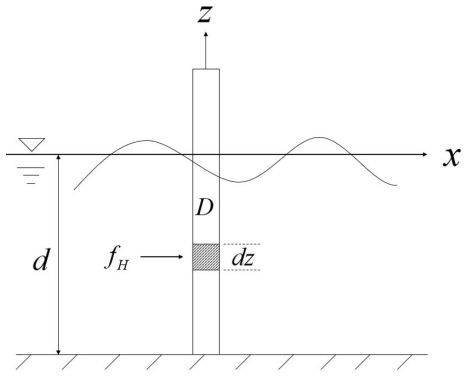

Fig. 1 The pile schematic

The acceleration water quality point movement at any height of z is expressed as:

$$\dot{u}_w = \frac{\partial u}{\partial t} = \frac{2\pi^2 H}{T^2}\frac{\cosh k\left(z+d\right)}{\sinh kd}\sin\left(kx-\omega t\right). \tag{4}$$

Let $kx - \omega t = \theta$, then it is substituted in Eqs. (4) and (5), and was integrated along the pile length, then the analytic solution of wave force can be acquired as shown in Eq. (5):

$$F_w = \rho C_D \frac{D}{2}\left(\frac{\pi H}{T\sinh kd}\right)^2 \int_0^d \cosh^2\left(kd\right)\left|\cos\theta\right|\cos\theta dz + \rho C_M \frac{\pi D^2}{4}\frac{2\pi^2 H}{T^2\sinh kd}\int_0^d \cosh kd\sin\theta dz. \tag{5}$$

Then simplification dispersion equation, the total wave force acting on the pile is obtained in Eq. (6):

$$F_w = \rho g V\left(\frac{H}{2d}\right)\tanh kd \times\left[C_D\frac{H}{4\pi D}\frac{2kd+\sinh kd}{\sinh^2 kd}\left|\cos\theta\right|\cos\theta + C_M\sin\theta\right], \tag{6}$$

where V is the pile volume submerged.

Based on Eq. (6), a wave force calculation program developed in Excel, which can calculate the wave force under different conditions, for wave heights of 1–5 m, wave periods of 5–9 s and water depths of 5–15 m, respectively, as shown from Fig. 2 to Fig.4.

2.2 Enhancing the load method in numerical

The AQUA is a specialized add-on module for ABAQUS, tailored for marine engineering applications. This module is capable of simulating the application of fluid inertia forces on structures, specifically by simulating steady-state currents and waves, which are defined by entering

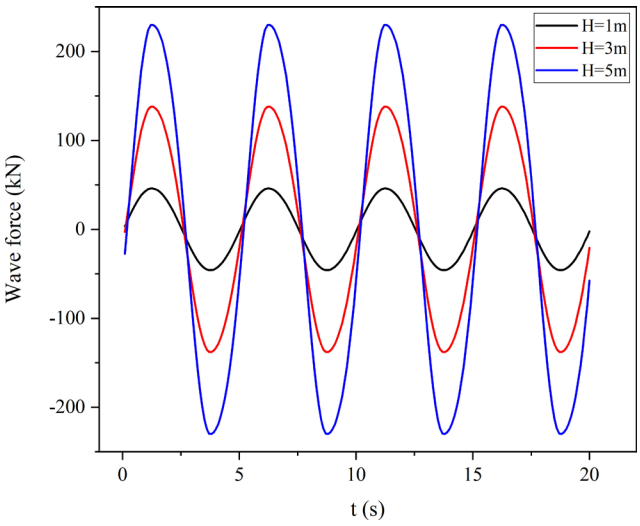

Fig. 2 The wave force in different wave heights

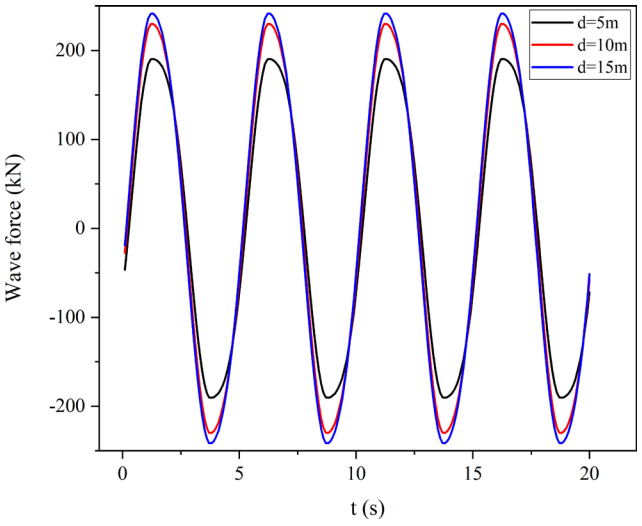

Fig. 3 The wave force in different water depths

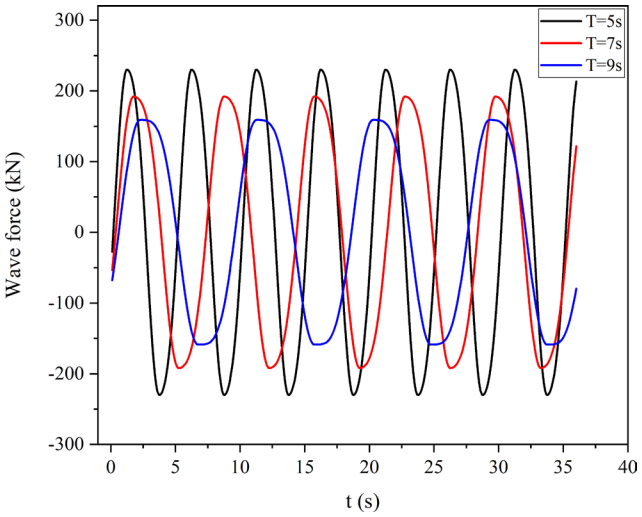

Fig. 4 The wave force in different wave periods

keywords within the ABAQUS software. Define the fluid parameters using the *AQUA keyword and wave parameters using the * wave keyword, then in *Dload define Drag and Inertia loads, respectively, then the wave force can be calculated in the ABAQUS.

A numerical model was developed, drawing upon the model test reported in a previous study [18]. The specifications of the test pile include a diameter of 0.05 m, a thickness of 5 mm, and a length of 1.1 m. The water depth was set at 0.6 m, the wave height was 0.12 m, and the period was 1.2 s. The pile was assumed to behave as a cantilever beam with a fixed tip, as depicted in Fig. 5. It was modeled as a linear elastic material with increased stiffness, the results obtained from the numerical model were found to align closely with those measured in the model test, specifically, the maximum measured wave force was 2.248 N, while the numerical result was 2.236 N, resulting in an error of only

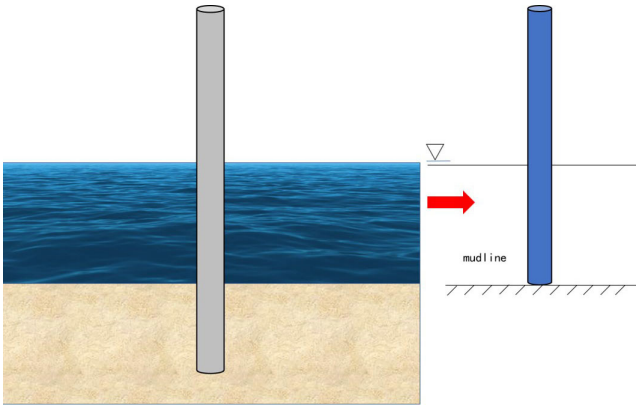

Fig. 5 The tip fixed model

0.68%, meanwhile, the wave force calculated using Eq. (6). The comparison demonstrates that the accuracy of wave force calculations in ABAQUS, as shown in Fig. 6.

3 The interactions between pile and soil under wave loading

3.1 Detailed description and rigorous validation of the model

The pile-soil model, depicted schematically in Fig. 7, illustrates a pile supported by the surrounding soil. The field test is introduced from the literature [19]. The finite element model presented in Fig. 8, features a soil length of 200 m and a height of 90 m, with parameters selected based on the sea area in Jiangsu Province, China, as detailed in Table 1. The performance of layered soil is evaluated using the Mohr-Coulomb model, with the pile modeled as having a diameter of 2 m, a length of 72.4 m, and a thickness of 28 mm. The interaction between the pile and soil is simulated using embedded region constraint.

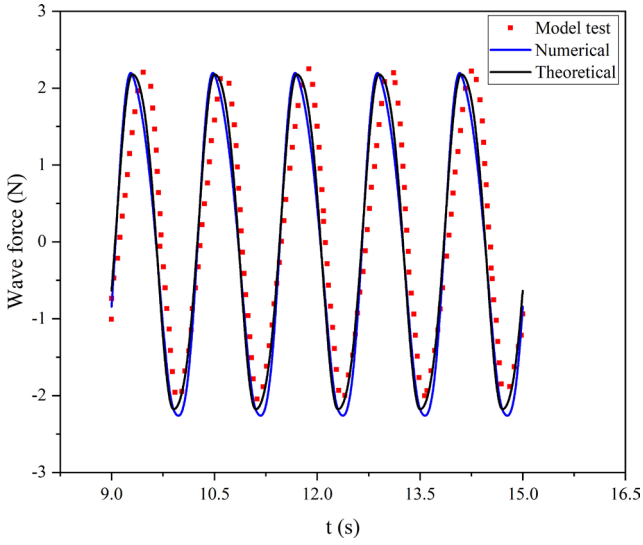

Fig. 6 Wave force in different methods

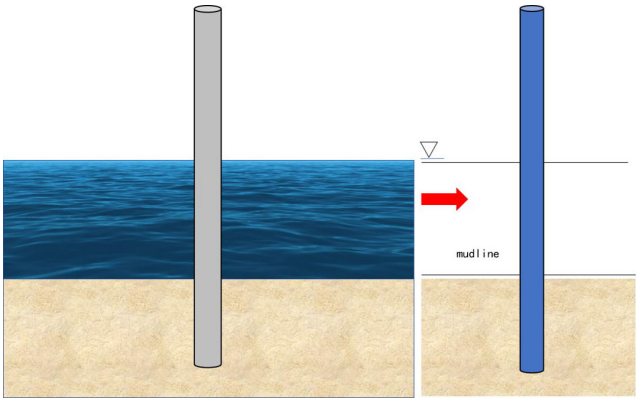

Fig. 7 The pile-soil model

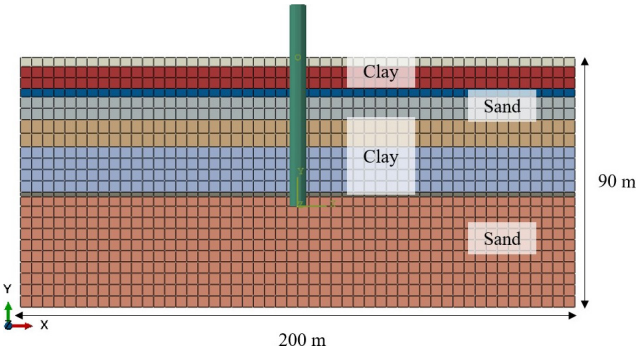

Fig. 8 The finite element model

Table 1 The layered soil parameters

Number	Layer	Depth (m)	γ (kN/m^3)	C (KPa)	φ (°)	v	E (MPa)
1	Clay	3.3	7.3	15	8.1	0.3	38.8
2	Clay	7.9	7.6	15	8.4	0.3	39.5
3	Sand	3	9	18	26.4	0.3	105.9
4	Sand	8.2	9.6	7	33.4	0.3	128.8
5	Clay	9.8	8.1	22	12.1	0.3	134.4
6	Clay	16.3	8.8	26	16.5	0.3	150.9
7	Clay	1.7	9.9	37	17.8	0.3	176.9
8	Sand	23.4	9.8	7	33.6	0.3	192.3

The study employs a single-cycle horizontal maintenance load method applied in one direction, with load levels of 250 kN, 500 kN, 600 kN, 700 kN, and 800 kN, respectively. The load-displacement curve and pile deflection curve compared with the field test results as shown in Fig. 9 and Fig. 10, the trends observed similar, but there are differences in the values, the reason for this is that the complexity of the soil, it is difficult to express all the soil properties in a model, so the results obtained through numerical simulation are similar in regularity to the field test, instead of completely consistent results. As the meshes were increased, the results showed minimal deviation, thereby validating the appropriateness of the mesh size selected for this study.

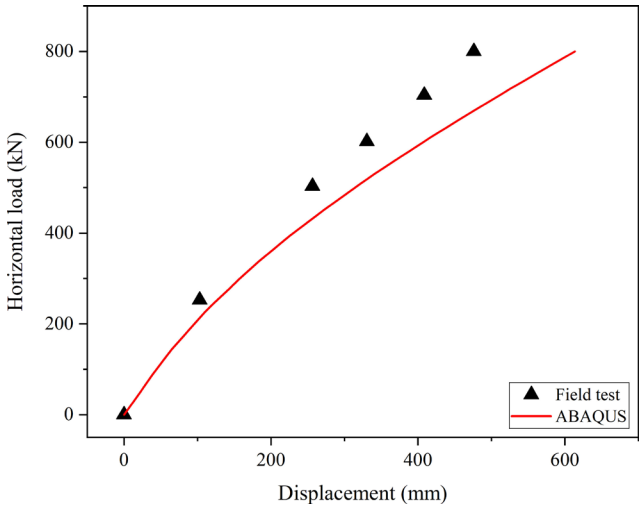

Fig. 9 The load-displacement

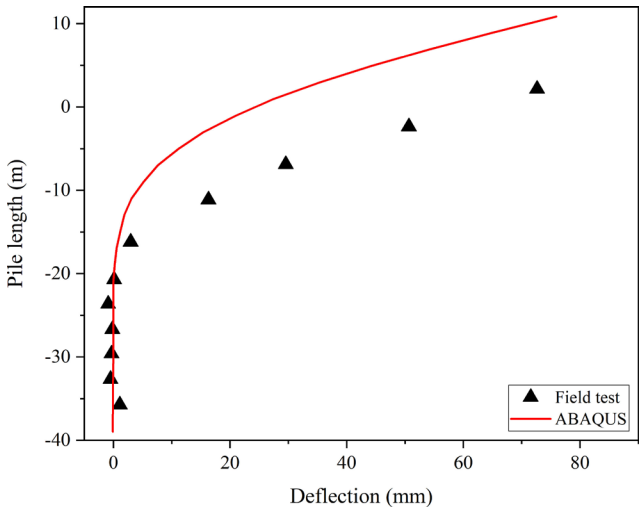

Fig. 10 The pile deflection

3.2 Analysis of soil plastic strain

After validating the finite element model, a pile with the diameter of 6 m, a length of 72.4 m, and a thickness of 75 mm was established, with the load applied as previously mentioned. It's crucial to note that the derivation of the Morison equation relies on the scenario of a rigid cylinder. Therefore, it's essential to assign the pile material property of high stiffness, ensuring that the deflection caused by deformation can be largely disregarded. The contour of soil plastic strain depicted in Fig. 11, it goes to show that the soil plastic strain mainly distributed in the clay layer, and the strain range increases with time, in the first of 0.06 s, the clay layer deeper at a depth of approximately 22.4 m below the mudline experiences the initial plastic strain, obviously, distributed on both sides of the pile, due to compression and tension respectively. The development becomes evident at 0.16 s, with the plastic strain initially expanding in the back of pile and gradually spreading outward, mainly because

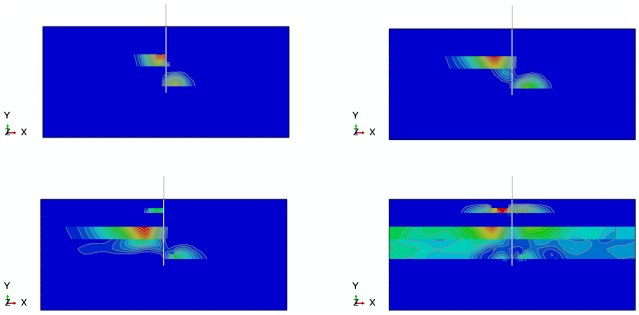

Fig. 11 The contour of soil plastic strain

wave loads increase with time. By 0.26 s, the wave loading continues to increase, the plastic strain towards to the shallow clay layer, meanwhile, expanding around. By the end of 10 s, the plastic strain distributed throughout the deeper clay layer and to a certain extent around the pile in the shallow layer. The findings reveal that the plastic strain primarily occurs in the clay layer, gradually increasing from the bottom up over time. The reason for that, when the horizontal load is small, the pile exhibits rigid characteristics, manifesting as rotation around a point, results in a significant increase of soil stress levels, and then a large deformation occurs, with the increasing loads, the pile exhibited different deformation behavior patterns, causes an increase in stress and deformation in the shallow layer. In addition, during the loading and unloading process of the wave action, clays soft and deformable nature compared to sandy soils, tend to compress their pores more readily, resulting in a higher pore pressure ratio, the excess pore pressure accumulated in the soil commences a gradual dissipation process when unloading.

The equivalent plastic strain serves as a metric for assessing soil plastic deformation, effectively documenting the soil's deformation history. This quantity characterizes cumulative plastic strain, with values exceeding zero indicating the occurrence of plastic strain. Fig. 12 illustrates that the plastic zone predominantly occurs within the clay layer, whereas the sand layer exhibits no cumulative plastic strain generation. This is attributed to the clay's plastic nature versus the sand's inelasticity, leading to plastic deformation primarily within the clay layer. The shallow soil remains resilient, generating no plastic strain. At a depth of 7.25 m, the plastic strain accumulates in front of and behind the pile, experiences plastic strain at 1.19 s and 5.2 s, as evident in Fig. 13, approximately peaking at 0.025% and 0.035%, respectively, this is due to the embedded pile-soil constraint, which exerts a tensile effect on the soil behind the pile during movement. Identifying the relationship between load and soil strain is straightforward.

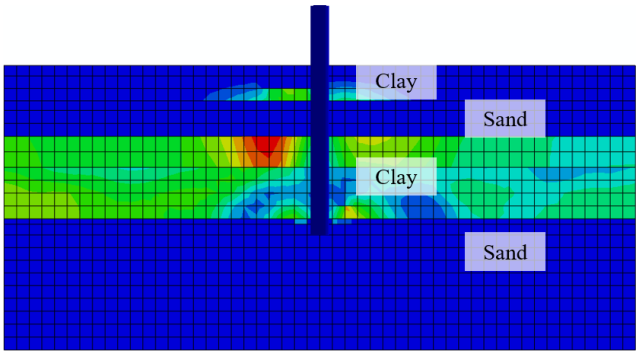

Fig. 12 The contour of soil PEEQ

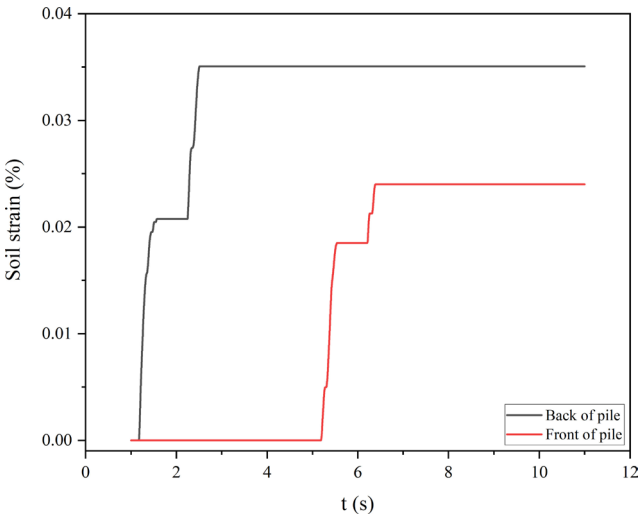

Fig. 13 The PEEQ in front and back of pile

3.3 Analysis of soil deformation

As depicted in Fig. 14, the soil deformation varies across different stages. It is crucial to comprehend the ground stress equilibrium for elucidating the initial stress that governs soil deformation. Prior to the application of wave forces, the pile-soil system is in a initial equilibrium state, characterized by tension in front of the pile and compression behind it at the mudline, with the opposite pattern observed at greater depths. Consequently, the deformation is minimal, exhibits a symmetrical displacement distribution with nearly zero values, as evident in Fig. 14 (a), the area extending 4 m to the left and right of the pile. Then, the soil displacement in front and back of pile as shown in Fig. 15, it is evident that the displacement curves are almost identical, ranging from −9.3 mm to 10.7 mm in front of the pile and from −9.7 mm to 10.4 mm behind it. These results suggest that, under wave loading, the displacement varies within a specific range, with different values at different times but similar trends on both sides of the pile. At a time of 5 s, the soil deformation contour as shown in Fig. 14 (b), compression is clearly observable

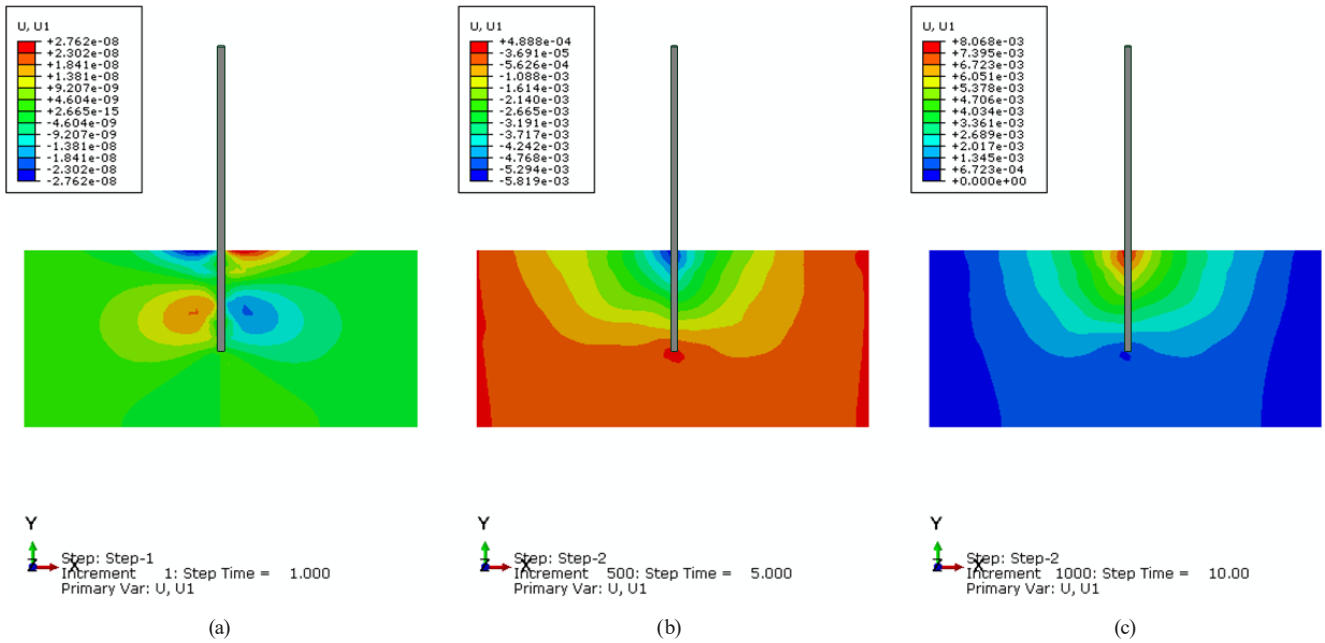

(a) (b) (c)

Fig. 14 The soil displacement in different steps; (a) initial state; (b) t = 5 s; (c) t = 10 s

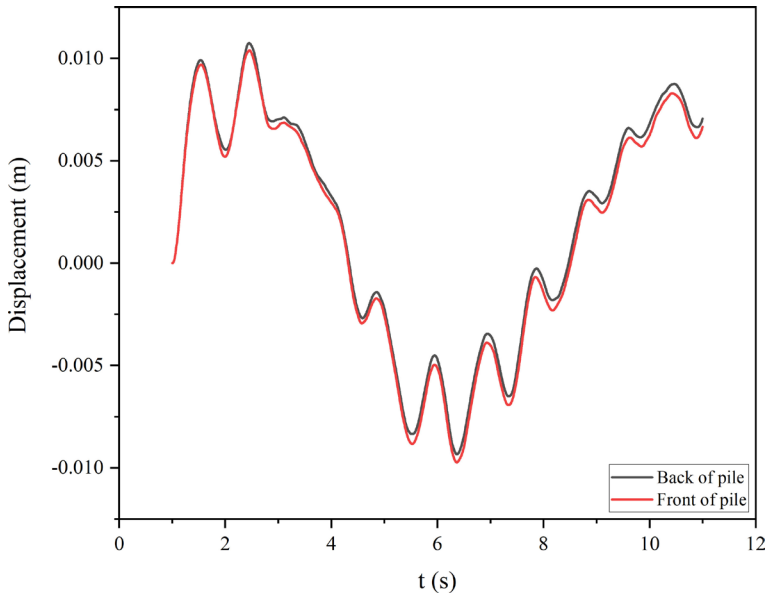

Fig. 15 The soil displacement changes with time

within a restricted zone encircling the pile at the mudline, gradually extending deeper in a tensile manner, the maximum displacement reaches −5.819 mm. At a time of 10 s, the observed result is diametrically opposed to 5 s, as shown in Fig. 14 (c), express as that tensile deformation near the pile at the mudline, while compression in the deeper, the maximum displacement increases to 8.068 mm. The main reason for that, the pile swings from one side to the other, at a time of 5 s, the pile oscillating along the negative direction of the x-axis under the wave loading, the embedded constraints suggest that the pile and soil are bonded, resulting in the soil moving with the pile under bonding action, thus causing negative displacement. The displacement observed at 10 s is greater than that at 5 s, which is attributed to the reduced bearing capacity of the soil resulting from accumulated deformation.

3.4 Analysis of soil stress

The pile swing under the wave loading causes constant loading and unloading of the surrounding soil, resulting in alterations in soil stress. These changes are primarily manifested as stress relief during unloading. Taking into account the initial stress of the soil, the stress variations can be determined by subtracting the final stress from the

initial stress, as depicted in Fig. 16, soil stresses exhibit a distinct periodic temporal variability, with fluctuations ranging from −15.25 kPa to 15.22 kPa in front of the pile and from −12.16 kPa to 18.25 kPa behind it, approximately symmetrically distributed. Notably, the patterns of soil stress variation in front and after the pile are inversely correlated, specifically, the peak stresses occur simultaneously at opposite locations, one in front and the other behind the pile. The reason for that the soil compression in front of the pile results in negative stress, whereas the tensile results in positive stress, concurrently, the observed transformation is precisely counter to the preceding trend. Since the pile is modeled as a beam embedded within the soil, it does not have direct contact with the soil, which inherently hinders the direct assessment of force transfer characteristics. However, based on the fundamental principle of force equilibrium, the force imposed by wave loading, with the pile tip constrained, can be equated to the reactive force from the surrounding soil. Using the wave forces calculated as mentioned earlier, the relationship between soil stress and wave force obtained as presented in Fig. 17, layers 1, 2, and 3, respectively representing the clay layer, the sand layer, and another clay layer. The results indicate a hysteresis curve trend in both. However, the sandy soil layer exhibits a smaller hysteresis circle compared to the clay layer. Furthermore, the hysteresis circle of the deep clay layer is notably larger than that of the shallow soil layer. The soil stress different with depths are depicted in Figs. 18 and 19, notably, the soil stress in the sand layer is the most significant, ranging from −21 kPa to 28.7 kPa behind the

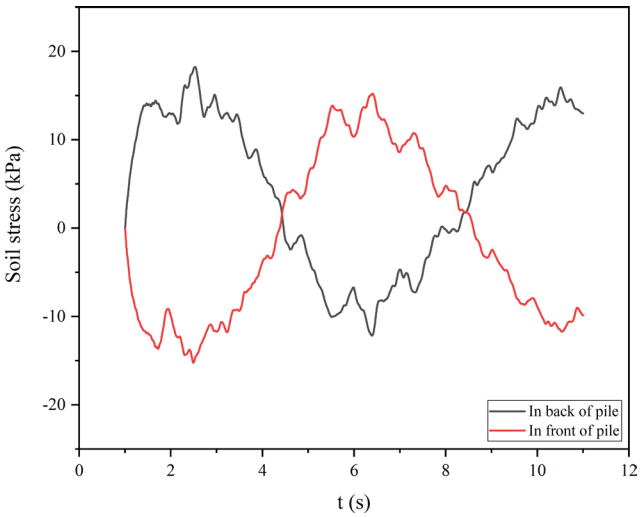

Fig. 16 The stress in the mudline

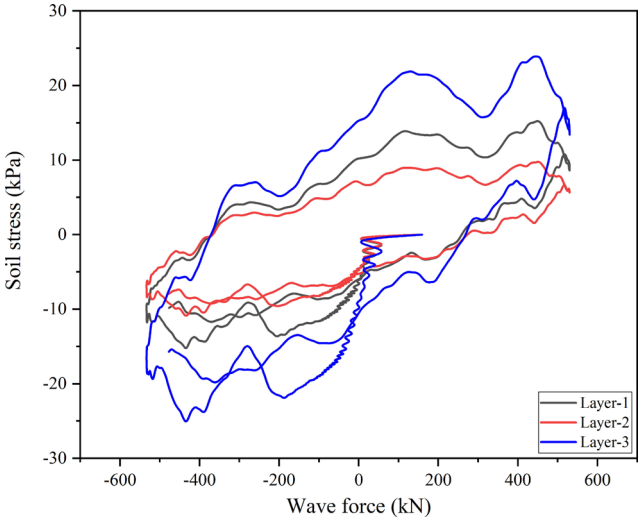

Fig. 17 The wave force and soil stress

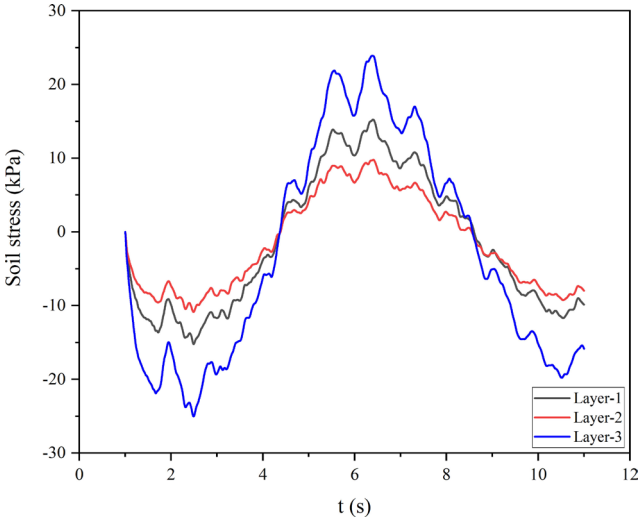

Fig. 18 The stress in front of pile

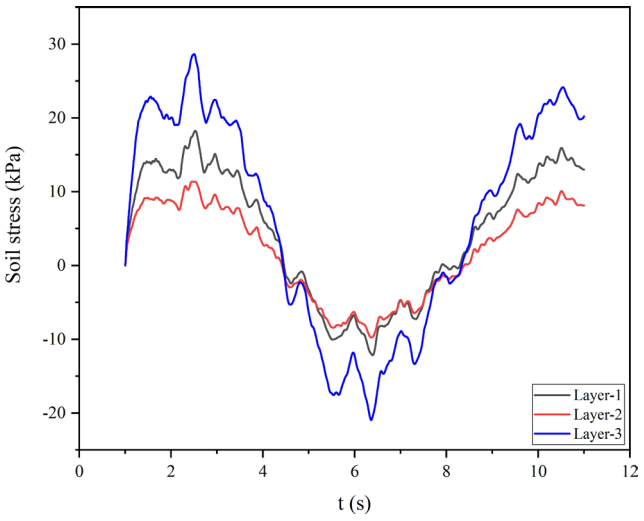

Fig. 19 The stress in back of pile

pile and from −25.1 kPa to 23.9 kPa in front. However, in the clay layer, the stress does not increase with depth, the maximum stress in front of the pile is 15.2 kPa in shallow layer, whereas it is 9.8 kPa in deeper layer. This occurs because sand exhibits elastic behavior, meaning that soil elastic strain recovers after unloading, whereas plastic strain in clay does not recover and accumulates upon reloading. These findings suggest that the clay layer's distribution along the depth significantly affects the soil stress. Therefore, it is crucial to consider layered soil configurations in the design process.

4 Conclusions

Based on the software of ABAQUS, a two-dimensional planar pile-soil model was established to investigate the pile-soil interaction under the wave loadings. The soil response was subsequently analyzed in detail. The main findings are as follows:

1. Under the wave loading, the large-diameter pile undergoes cyclic reciprocating motion, the soil displacement pattern surrounding the pile remains consistent before and after, a positive correlation between pile foundation displacement and wave force, the plastic strain primarily occurs in the clay layer, gradually increasing from the bottom up over time.
2. The pile-soil interaction under wave loading exhibits a distinct cyclic trend, characterized by the displacement and strain, the displacement ranging from −9.3 mm to 10.7 mm in front of the pile and from −9.7 mm to 10.4 mm. The plastic strain initially arises in the soil proximate to the point of rotation, rather than at the mudline. When the load is minimal, it originates near the rotation point and gradually spreads towards the mudline and encompassing soil as the load intensifies.
3. The majority of plastic strain occurring within the clay layer under the wave loading. The presence of a larger friction angle in sandy soil gives rise to pronounced interactions among soil particles, leading to a more significant stress path in the sand layer compared to the clay layer. The maximum stress is 23.9 kPa in sand layer, while 15.2 kPa in clay layer. The stress does not correlate with depth in the clay layer, but significantly influenced by the clay layer's distribution.

References

[1] Oh, K.-Y., Nam, W., Ryu, M. S., Kim, J.-Y., Epureanu, B. I. "A review of foundations of offshore wind energy convertors: Current status and future perspectives", Renewable and Sustainable Energy Reviews, 88, pp. 16–36, 2018. https://doi.org/10.1016/j.rser.2018.02.005

[2] Govindasamy, V. K., Chella, M. A., Sannasi Annamalaisamy, S., Rajamanickam, P. S. "Impact pressure distribution and characteristics of breaking wave impact on a monopile", Ocean Engineering, 271, 113771, 2023. https://doi.org/10.1016/j.oceaneng.2023.113771

[3] Pákozdi, C., Kamath, A., Wang, W., Bihs, H. "Application of Arbitrary Lagrangian-Eulerian strips with fully nonlinear wave kinematics for force estimation", Marine Structures, 83, 103190, 2022. https://doi.org/10.1016/j.marstruc.2022.103190

[4] Ullah, Z., Choi, D.-H. "On the Hydrostatic Nonlinearity of Spar Type Floating Offshore Wind Turbine", In: Proceedings of the 17th Biennial International Conference on Engineering, Science, Construction, and Operations in Challenging Environments (Earth and Space 2021), [webinar], 2021, pp. 464–475. ISBN 9780784483381 https://doi.org/10.1061/9780784483381.043

[5] Liu, C., Zhang, Q., Li, M., Li, W. "波浪与地震荷载共同作用下桩的动力响应" (Dynamic Response of Pile at Waterwave Load and Seismic Load), Journal of Shanghai Jiao Tong University, 55(6), pp. 638–644, 2021. (in Chinese) https://doi.org/10.16183/j.cnki.jsjtu.2020.142

[6] Kimmoun, L., Brosset, L. "Assessment of the Morison Equation for Nonimpacting Wave Loads on a Vertical Cylinder", International Journal of Offshore and Polar Engineering, 33(1), pp. 36–46, 2023. https://doi.org/10.17736/ijope.2023.mk75

[7] Zdravković, L., Taborda, D. M. G., Potts, D. M., Abadias, D., Burd, H. J., Byrne, B. W., Gavin, K. G., … Ushev, E. "Finite-element modelling of laterally loaded piles in a stiff glacial clay till at Cowden", Géotechnique, 70(11), pp. 999–1013, 2020. https://doi.org/10.1680/jgeot.18.PISA.005

[8] Taborda, D. M. G., Zdravković, L., Potts, D. M., Burd, H. J., Byrne, B. W., Gavin, K. G., Houlsby, G. T., … McAdam, R. A. "Finite-element modelling of laterally loaded piles in a dense marine sand at Dunkirk", Géotechnique, 70(11), pp. 1014–1029, 2020. https://doi.org/10.1680/jgeot.18.PISA.006

[9] Asumadu, R., Zhang, J.-S., Hubert, O.-W.., Akoto, A. B. "Two-dimensional model of wave-induced response of seabed around permeable submerged breakwater", Advances in Mechanical Engineering, 11(3), 1687814019830809, 2019. https://doi.org/10.1177/1687814019830809

[10] Asumadu, R., Zhang, J., Osei-Wusuansa, H. "3-D numerical study of offshore tripod wind turbine pile foundation on wave-induced seabed response", Ocean Engineering, 255, 111421, 2022. https://doi.org/10.1016/j.oceaneng.2022.111421

[11] Asumadu, R., Zhang, J., Zhao, H. Y., Osei-Wusuansa, H., Akoto, A. B. "3-Dimensional numerical study of wave-induced seabed response around three different types of wind turbine pile foundations", SN Applied Sciences, 1(11), 1401, 2019. https://doi.org/10.1007/s42452-019-1484-2

[12] Zhao, H. Y., Jeng, D.-S., Liao, C. C., Zhu, J. F. "Three-dimensional modeling of wave-induced residual seabed response around a mono-pile foundation", Coastal Engineering, 128, pp. 1–21, 2017. https://doi.org/10.1016/j.coastaleng.2017.07.002

[13] Wang, G., Liu, Q., Zhang, Y. "波浪荷载作用下海床的液化及参数分析" (Momentary liquefaction and parametric analysis of seabed under wave loadings), Journal of Zheijang University of Technology (China), 47(2), pp. 135–139, 145, 2019. (in Chinese) https://doi.org/10.3969/j.issn.1006-4303.2019.02.004

[14] Abhinav, K. A., Saha, N. "Nonlinear dynamical behaviour of jacket supported offshore wind turbines in loose sand", Marine Structures, 57, pp. 133–151, 2018. https://doi.org/10.1016/j.marstruc.2017.10.002

[15] Guo, J., Zhou, X., Xu, F., Wang, J. "Wave-Induced Dynamic Response of Seabed and Pile", Journal of Shanghai Jiao Tong University, 50(11), pp. 1694–1699, 2016. https://doi.org/10.16183/j.cnki.jsjtu.2016.11.006

[16] Liu, H., Sun, P., Hu, R., Cao, L. "波浪荷载作用下单桩基础桩周土体的应力位移分析" (Displacement and stress of soil around the single pile foundation under wave loading), Periodical of Ocean University of China, 1(Supp.), pp. 137–144, 2020. (in Chinese) https://doi.org/10.16441/j.cnki.hdxb.20180402

[17] Morison J. R., Johnson J. W., Schaaf, S. A. "The Force Exerted by Surface Waves on Piles", Journal of Petroleum Technology, 2(05), pp. 149–154, 1950. https://doi.org/10.2118/950149-g

[18] Lan, Y. "桩基结构物的波-流作用力研究" (Studies on Hydrodynamic Loads on Piled Structures in Wave-current Combination), PhD Thesis, Shanghai Jiao Tong University, 2006. (in Chinese)

[19] Xu, H., Lyu, P., Du, X. "基于现场试验的海上风电大直径单桩三维水平承载力研究" (Research on 3D horizontal bearing capacity of large diameter monopile of offshore wind power based on field test), Water Resources and Hydropower Engineering, 51(7), pp. 154–160, 2021. (in Chinese) https://doi.org/10.13928/j.cnki.wrahe.2020.07.020